Editors' Suggestion | Featured in Physics

First Measurement of ν_e and ν_μ Interaction Cross Sections at the LHC with FASER's Emulsion Detector

Roshan Mammen Abraham,[1] John Anders,[2] Claire Antel,[3] Akitaka Ariga,[4,5] Tomoko Ariga,[6,*] Jeremy Atkinson,[4] Florian U. Bernlochner,[7] Tobias Boeckh,[7] Jamie Boyd,[2] Lydia Brenner,[8] Angela Burger,[2] Franck Cadoux,[3] Roberto Cardella,[3] David W. Casper,[1] Charlotte Cavanagh,[9] Xin Chen,[10] Andrea Coccaro,[11] Stephane Débieux,[3] Monica D'Onofrio,[9] Ansh Desai,[12] Sergey Dmitrievsky,[13] Sinead Eley,[9] Yannick Favre,[3] Deion Fellers,[12] Jonathan L. Feng,[1] Carlo Alberto Fenoglio,[3] Didier Ferrere,[3] Max Fieg,[1] Wissal Filali,[7] Haruhi Fujimori,[5] Ali Garabaglu,[14] Stephen Gibson,[15] Sergio Gonzalez-Sevilla,[3] Yuri Gornushkin,[13] Carl Gwilliam,[9] Daiki Hayakawa,[5] Shih-Chieh Hsu,[14] Zhen Hu,[10] Giuseppe Iacobucci,[3] Tomohiro Inada,[2] Luca Iodice,[3] Sune Jakobsen,[2] Hans Joos,[2,16] Enrique Kajomovitz,[17] Takumi Kanai,[5] Hiroaki Kawahara,[6] Alex Keyken,[15] Felix Kling,[18] Daniela Köck,[12] Pantelis Kontaxakis,[3] Umut Kose,[19] Rafaella Kotitsa,[2] Susanne Kuehn,[2] Thanushan Kugathasan,[3] Helena Lefebvre,[15] Lorne Levinson,[20] Ke Li,[14] Jinfeng Liu,[10] Margaret S. Lutz,[2] Jack MacDonald,[21] Chiara Magliocca,[3] Fulvio Martinelli,[3] Lawson McCoy,[1] Josh McFayden,[22] Andrea Pizarro Medina,[3] Matteo Milanesio,[3] Théo Moretti,[3] Magdalena Munker,[3] Mitsuhiro Nakamura,[23] Toshiyuki Nakano,[23] Friedemann Neuhaus,[21] Laurie Nevay,[2] Motoya Nonaka,[5] Kazuaki Okui,[5] Ken Ohashi,[4] Hidetoshi Otono,[6] Hao Pang,[10] Lorenzo Paolozzi,[3,2] Brian Petersen,[2] Markus Prim,[7] Michaela Queitsch-Maitland,[24] Hiroki Rokujo,[23] Elisa Ruiz-Choliz,[21] André Rubbia,[19] Jorge Sabater-Iglesias,[3] Osamu Sato,[23] Paola Scampoli,[4,25] Kristof Schmieden,[21] Matthias Schott,[21] Anna Sfyrla,[3] Mansoora Shamim,[2] Savannah Shively,[1] Yosuke Takubo,[26] Noshin Tarannum,[3] Ondrej Theiner,[3] Eric Torrence,[12] Svetlana Vasina,[13] Benedikt Vormwald,[2] Di Wang,[10] Yuxiao Wang,[10] Eli Welch,[1] Samuel Zahorec,[2,27] Stefano Zambito,[3] and Shunliang Zhang[10]

(FASER Collaboration)[†]

[1]*Department of Physics and Astronomy, University of California, Irvine, California 92697-4575, USA*
[2]*CERN, CH-1211 Geneva 23, Switzerland*
[3]*Département de Physique Nucléaire et Corpusculaire, University of Geneva, CH-1211 Geneva 4, Switzerland*
[4]*Albert Einstein Center for Fundamental Physics, Laboratory for High Energy Physics, University of Bern, Sidlerstrasse 5, CH-3012 Bern, Switzerland*
[5]*Department of Physics, Chiba University, 1-33 Yayoi-cho Inage-ku, 263-8522 Chiba, Japan*
[6]*Kyushu University, Nishi-ku, 819-0395 Fukuoka, Japan*
[7]*Universität Bonn, Regina-Pacis-Weg 3, D-53113 Bonn, Germany*
[8]*Nikhef National Institute for Subatomic Physics, Science Park 105, 1098 XG Amsterdam, Netherlands*
[9]*University of Liverpool, Liverpool L69 3BX, United Kingdom*
[10]*Department of Physics, Tsinghua University, Beijing, China*
[11]*INFN Sezione di Genova, Via Dodecaneso, 33–16146, Genova, Italy*
[12]*University of Oregon, Eugene, Oregon 97403, USA*
[13]*Affiliated with an international laboratory covered by a cooperation agreement with CERN*
[14]*Department of Physics, University of Washington, P.O. Box 351560, Seattle, Washington 98195-1460, USA*
[15]*Royal Holloway, University of London, Egham, TW20 0EX, United Kingdom*
[16]*II. Physikalisches Institut, Universität Göttingen, Göttingen, Germany*
[17]*Department of Physics and Astronomy, Technion—Israel Institute of Technology, Haifa 32000, Israel*
[18]*Deutsches Elektronen-Synchrotron DESY, Notkestrasse 85, 22607 Hamburg, Germany*
[19]*ETH Zurich, 8092 Zurich, Switzerland*
[20]*Department of Particle Physics and Astrophysics, Weizmann Institute of Science, Rehovot 76100, Israel*
[21]*Institut für Physik, Universität Mainz, Mainz, Germany*
[22]*Department of Physics and Astronomy, University of Sussex, Sussex House, Falmer, Brighton, BN1 9RH, United Kingdom*
[23]*Nagoya University, Furo-cho, Chikusa-ku, Nagoya 464-8602, Japan*
[24]*School of Physics and Astronomy, Schuster Building, University of Manchester, Oxford Road, Manchester M13 9PL, United Kingdom*
[25]*Dipartimento di Fisica "Ettore Pancini," Università di Napoli Federico II, Complesso Universitario di Monte S. Angelo, I-80126 Napoli, Italy*

[26]Institute of Particle and Nuclear Studies, KEK, Oho 1-1, Tsukuba, Ibaraki 305-0801, Japan
[27]Faculty of Mathematics and Physics, Charles University, Prague, Czech Republic

(Received 22 March 2024; accepted 28 May 2024; published 11 July 2024)

The first results of the study of high-energy electron neutrino (ν_e) and muon neutrino (ν_μ) charged-current interactions in the FASERν emulsion-tungsten detector of the FASER experiment at the LHC are presented. A 128.8 kg subset of the FASERν volume was analyzed after exposure to 9.5 fb^{-1} of $\sqrt{s} = 13.6$ TeV pp data. Four (eight) ν_e (ν_μ) interaction candidate events are observed with a statistical significance of 5.2σ (5.7σ). This is the first direct observation of ν_e interactions at a particle collider and includes the highest-energy ν_e and ν_μ ever detected from an artificial source. The interaction cross section per nucleon σ/E_ν is measured over an energy range of 560–1740 GeV (520–1760 GeV) for ν_e (ν_μ) to be $(1.2^{+0.8}_{-0.7}) \times 10^{-38}$ cm^2 GeV^{-1} $[(0.5 \pm 0.2) \times 10^{-38}$ cm^2 GeV$^{-1}]$, consistent with standard model predictions. These are the first measurements of neutrino interaction cross sections in those energy ranges.

DOI: 10.1103/PhysRevLett.133.021802

Introduction.—To date, neutrino interaction cross sections have not been measured at energies above 300 GeV for ν_e and between 400 GeV and 6 TeV for ν_μ. One of the primary physics goals of FASER [1–3], the Forward Search Experiment at CERN's Large Hadron Collider (LHC) [4], is the study of high-energy neutrinos produced in the LHC's proton-proton (pp) collisions using the dedicated FASERν detector [5,6]. FASERν is a tungsten-emulsion detector that is located in front of the FASER spectrometer [7]. With FASERν, charged particle tracks produced by neutrino interactions in the detector can be reconstructed with submicron precision. This allows us to identify leptons and measure the energies of electrons and momenta of muons, enabling the identification of electron and muon charged-current (CC) neutrino interactions and the measurement of neutrino interaction cross sections in the currently unexplored TeV energy range. In this study, we do not measure the charge of the outgoing charged leptons; charge conjugation is implied, and $\nu_{e/\mu}$ represents the sum of both $\nu_{e/\mu}$ and $\bar{\nu}_{e/\mu}$.

The decays of hadrons originating from LHC pp collisions produce a large number of neutrinos, which are focused along the beam collision axis or line of sight (LOS). Neutrinos close to the LOS are characterized by very high energies up to several TeV, and they therefore have relatively large interaction cross sections. Since neutrinos only interact weakly, they are not affected by the 100 m of rock or by the magnetic fields between the collision point and the detector. These, however, substantially reduce the rate of background particles.

The first evidence for neutrino interaction candidates produced at the LHC was reported by the FASER Collaboration in 2021 [8]. The first observation of muon neutrinos by means of the FASER electronic detector components was achieved in 2023 [9]. The SND@LHC Collaboration [10,11] confirmed this observation in Ref. [12], studying a different rapidity region. Nevertheless, to date no electron neutrino has ever been directly detected at the LHC.

Neutrinos interact through $\nu_e + N \to e^- + X$ (ν_e CC events), $\nu_\mu + N \to \mu^- + X$ (ν_μ CC events), $\nu_\tau + N \to \tau^- + X$ (ν_τ CC events) [13], and $\nu_l + N \to \nu_l + X$ ($l = e,\ \mu,\ \tau$) [neutral-current (NC) events], where N represents a nucleon in the tungsten target, and X represents interaction products. At FASER, the main background to neutrino detection arises from neutral hadrons interacting in the detector. These neutral hadrons are generally lower in energy than the neutrino signal, and they can therefore be suppressed with appropriate selections on topological and kinematic variables related to the reconstructed interaction vertices. The additional requirement of a high-energy electron or muon signature further suppresses this background and allows us to distinguish ν_e and ν_μ CC interactions.

The current analysis is the first step of a broad physics program on neutrino measurements at the LHC, which will provide important insights in neutrino and electroweak physics, as well as in quantum chromodynamics by probing forward hadron production and the deep inelastic scattering of high-energy neutrinos, as detailed in Refs. [14–18].

The FASERν *detector and data taking.*—The FASERν emulsion detector is made of 730 layers of interleaved tungsten plates and emulsion films [19], with a total target mass of 1.1 metric tons. The tungsten plates are 1.1 mm thick, and each emulsion film is 0.34 mm thick. The detector is 1.05 m long and has a transverse area with respect to the neutrino beam of 25×30 cm^2. The detector is aligned with the LOS and placed in front of the FASER spectrometer, 480 m away from the pp collision point

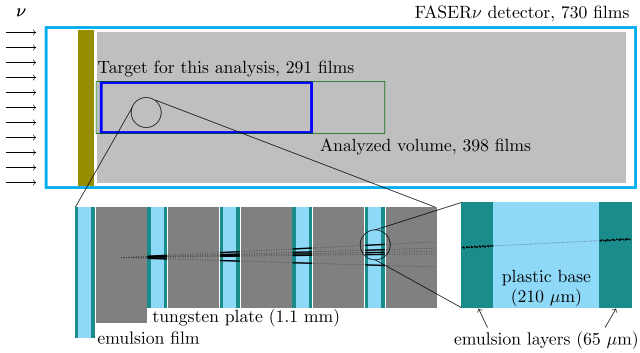

FIG. 1. Schematic view of the analyzed detector volume (side view). The FASERν box contains a total of 730 emulsion films and is shown in gray. The thin green box outlines the reconstructed volume, and neutrino interactions are searched for within the fiducial volume defined by the blue box.

within the ATLAS experiment (IP1). A more detailed description of the FASERν detector is provided in Ref. [7].

The analyzed dataset was collected between July 26 and September 13, 2022, corresponding to 9.5 fb^{-1} of pp collisions at a center-of-mass energy of 13.6 TeV. The integrated luminosity is measured by the ATLAS experiment [20–22] with an uncertainty of 2.2%. For the analysis presented in this Letter, only 14% of the detector volume, shown in Fig. 1, is considered as the target region for neutrino interaction vertices. In the transverse [23] (x-y) plane, a region of 23.4×9.0 cm^2 is analyzed, and in the longitudinal direction, 41.5 cm, including 31.6 cm of tungsten (291 tungsten plates), is considered. The corresponding target mass is 128.6 kg. Data from seven films upstream of the target region are used to check the absence of charged parent tracks. Data from an additional 100 plates immediately downstream of the target region are used to measure the energy or the momentum of the particle tracks. The LOS passes through the center of the analyzed volume in the horizontal plane and about 2 cm from the bottom in the vertical plane.

After chemical development, the emulsion films are read out by the Hyper Track Selector (HTS) system [24]. The HTS system divides each emulsion film into eight readout zones. A multistage alignment procedure is used. The first alignment between each two consecutive films is performed using the recorded track hits for each readout zone. The data are then divided into subvolumes of 1.7 cm $\times$ 1.7 cm $\times$ 15 films due to limitations in memory usage and to achieve a better alignment resolution. After a second alignment between each two consecutive films and track reconstruction in each subvolume, an additional alignment is applied by selecting those tracks crossing 15 plates to improve the tracking resolution. Finally, the track reconstruction procedure [25] links track hits on different films by correlating their positions and angles.

Simulation samples.—Monte Carlo (MC) samples for neutrino and background processes are used to define the event selection criteria, to estimate the backgrounds, and to assess systematic uncertainties.

The neutrino energy spectra, relative flavor composition, and transverse spatial distribution are simulated as follows. The neutrino fluxes are obtained using the fast neutrino flux simulation introduced in Ref. [26]. As described in Ref. [27], light hadrons (pions, kaons, and hyperons) are simulated using EPOS-LHC [28], QGSJET II-04 [29], SIBYLL2.3d, and PYTHIA8 [30] with a forward physics tune [31]. EPOS-LHC is used as the baseline flux model, with the envelope of the considered models used to determine the systematic uncertainty. Charm hadrons are simulated using POWHEG+PYTHIA8 [32]. In Ref. [32], the uncertainty is considered by varying the renormalization and factorization scale by a factor of 2. The interaction of neutrinos with the tungsten-emulsion detector is simulated using the GENIE event generator [33,34]. The interactions of all other particles traversing the tungsten-emulsion detector are simulated using GEANT4 [35]. In the default setup, the FTFP_BERT physics list is used to model hadron interactions.

The main background contributions arise from neutral hadrons produced in the photonuclear interactions of muons within the rock in front of the FASER detector or within the FASERν detector material. The muon flux is measured to be $(1.43 \pm 0.07) \times 10^4$ tracks/cm^2/fb^{-1}, as estimated from the reconstructed tracks within an angle of $\Delta\theta < 10$ mrad from the beam direction in the FASERν detector. The neutral-hadron background is simulated through a multistep process. First, the energy spectrum of muons is simulated using the FLUKA package [36,37], which includes a detailed model of the LHC infrastructure between IP1 and FASER. GEANT4 was then used to simulate the interactions of these muons within the rock in front of FASER or in the tungsten of the FASERν detector. Finally, high-statistics samples of the individual neutral-hadron species (K_S, K_L, n, Λ, $\bar{n}$, and $\bar{\Lambda}$) were produced and weighted to follow the expected energy spectra estimated by the previous step.

The simulated events are reconstructed in the same way as the data. Corrections are applied to the simulated samples to reproduce the hit efficiencies, position, and angular resolutions of the data.

Event reconstruction and selection.—Candidate ν_e and ν_μ CC interactions are selected based on reconstructed charged particle tracks, forming a neutral vertex in FASERν. The number of neutral hadrons drops quickly with increasing energy. Since neutrinos are more energetic than the neutral-hadron background, the tracks associated with the vertex are boosted in the forward direction. A CC interaction produces a high-energy electron or muon, well separated in azimuthal angle from the other particles associated with the vertex.

Vertex selection: Using the reconstructed tracks passing through at least three plates, the vertex reconstruction is

performed by searching for converging track patterns with an impact parameter less than 5 μm. Tracks with $\tan\theta \leq 0.5$ are retained, and converging patterns with more than four tracks are selected as vertices. The tracks are required to start within three films downstream of the vertices. The number of tracks with $\tan\theta \leq 0.1$ relative to the beam direction is also required to be greater than 3 to suppress the neutral-hadron background. Furthermore, the vertices are required to not have a parent track.

Electron identification and energy measurement: Candidate ν_e CC interactions are selected from the initial set of vertices by requesting an associated high-energy electromagnetic (EM) shower with a reconstructed energy above 200 GeV and $\tan\theta > 0.005$. The latter requirement is used to reduce the neutral-hadron background. It improves the signal-to-noise ratio because leptons from neutrino CC interactions have larger angles, due to higher transverse momenta, than high-energy particles from the neutral hadron background. The EM shower is required to start within two films downstream of the vertices. The EM shower must have an azimuthal angle, relative to the sum of all other tracks in the vertex, $\Delta\phi > \pi/2$. This cut is motivated by the expectation that, for CC interactions, the outgoing lepton and hadrons are back to back in the transverse plane.

The EM shower is formed by reconstructed tracks in the emulsion, produced from electron-positron pair production as the shower develops [38,39]. Given the short radiation length of tungsten, the EM shower remains compact and can be associated with the vertex. The EM shower reconstruction is based on searching for track segments in a cylinder of radius 100 μm around the shower axis, defined by iteratively fitting the group of segments belonging to the shower. The algorithm selections were defined using the profile of EM showers from electrons with energy above 200 GeV in simulation and that of background showers in data and simulation. The number of track segments in ±3 films around the shower maximum (seven films in total), which we denote $N_{\rm seg}$, is used to identify EM showers and estimate the electron energy. Several selections on the track segment position and angle with respect to the shower axis are applied to reduce the contribution from background segments not associated with the EM shower. Additionally, the average residual background is estimated by using randomly positioned cylinders, whose average number of segments, $N_{\rm seg}^{\rm bg}$ is then subtracted from the shower before the energy is estimated. The energy reconstruction is performed using the relation between the difference $N_{\rm seg} - N_{\rm seg}^{\rm bg}$ and electron energy which is fitted with a polynomial, as defined with simulation. The energy reconstruction algorithm performance was tested for electrons in the ν_e MC simulation, showing a resolution of around 25% at 200 GeV and between 25% and 40% at higher energies.

Muon identification and momentum measurement: Candidate ν_μ CC interactions are selected from the initial set of vertices by requiring that one of the reconstructed charged particle tracks associated with the vertex is a muon candidate. Muon candidates are defined as tracks that penetrate more than 100 tungsten plates without exhibiting secondary hadron interactions consisting of at least two daughter tracks. Furthermore, the muon reconstructed momentum p has to be greater than 200 GeV with $\tan\theta > 0.005$. Simulation studies show that the probability for a charged hadron with $p > 200$ GeV to satisfy the muon candidate requirements is about 20%. The muon candidate track is then required to have an azimuthal angle $\Delta\phi > \pi/2$.

The track momentum is estimated by measuring multiple Coulomb scattering using the so-called coordinate method [40]. The performance of the momentum evaluation algorithm is studied using simulated muon tracks with a flat momentum distribution from 1 to 2000 GeV, including position and angular smearing to account for residual misalignments between the emulsion films. The resolution, as quantified by the rms of the distribution of the difference between the true momentum and reconstructed momentum, is around 30% at 200 GeV and reaches 50% at higher energies.

Selection efficiencies and systematic uncertainties: The selection efficiencies for ν_e CC, $\bar{\nu}_e$ CC, ν_μ CC, and $\bar{\nu}_\mu$ CC events are shown in Fig. 2. Because of the helicity combination, leptons in antineutrino events are more boosted, and the other particles have less energy, than in neutrino events. Consequently, the efficiency of antineutrino events to pass the vertex selection is slightly lower than that of neutrino events.

Systematic uncertainties related to the signal expectation are summarized in Table I. The systematic uncertainty from

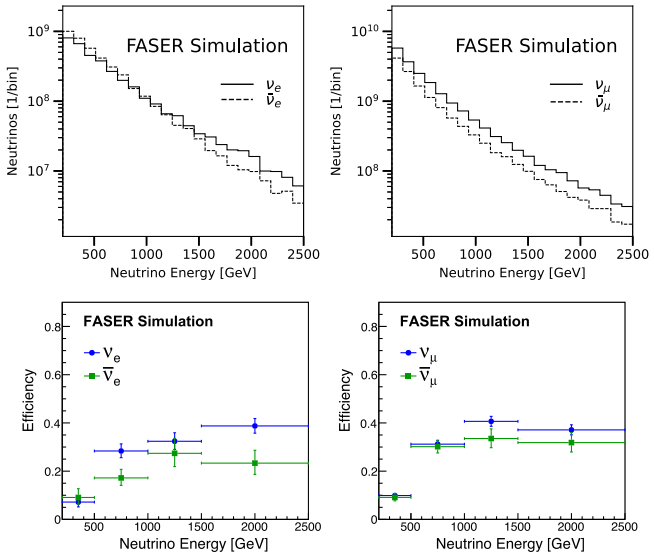

FIG. 2. Top: simulation of the fluxes for ν_e and $\bar{\nu}_e$ (left) and for ν_μ and $\bar{\nu}_\mu$ (right). Bottom: selection efficiencies for ν_e CC and $\bar{\nu}_e$ CC interactions (left) and for ν_μ CC and $\bar{\nu}_\mu$ CC interactions (right). The statistical uncertainties are shown.

TABLE I. Systematic uncertainties related to the signal expectation.

Source	Relative uncertainty ν_e (%)	ν_μ (%)
Luminosity	2.2	2.2
Tungsten thickness	1	1
Interactions with emulsions	$^{+3.6}_{-0}$	$^{+3.6}_{-0}$
Flux uncertainty	$^{+70}_{-22}$	$^{+16}_{-9}$
Line of sight position	$^{+2.1}_{-2.4}$	$^{+1.9}_{-2.5}$
Efficiency from hadronization	$^{+22}_{-5}$	$^{+23}_{-5}$
Efficiency from reconstruction	20	20
Efficiency from MC statistics	4.9	2.8
Total	$^{+70}_{-22}$ (flux) $^{+30}_{-21}$ (other)	$^{+16}_{-9}$ (flux) $^{+31}_{-21}$ (other)

TABLE II. The number of MC reconstructed events of neutral-hadron interactions satisfying the ν_e and ν_μ CC event selection. The scaling factor shows the ratio of the data luminosity to the MC luminosity.

Hadron type	K_L	n	Λ
Events simulated ($E_h > 200$ GeV)	13 497	13 191	13 902
Events selected as ν_e CC	0	0	0
Events selected as ν_μ CC	6	11	5
Scaling factor (data/MC)	1/232	1/256	1/423
Hadron type	K_S	$\bar{n}$	$\bar{\Lambda}$
Events reconstructed ($E_h > 200$ GeV)	7113	5827	5368
Events selected as ν_e CC	1	0	0
Events selected as ν_μ CC	3	3	4
Scaling factor (data/MC)	1/436	1/569	1/630

tungsten thickness is estimated based on the variation of the measured plate thickness. The systematic uncertainty from the LOS position is estimated by varying the detector alignment with the LOS by ± 1 cm. The systematic uncertainty from hadronization in the neutrino interaction simulation is estimated using five different PYTHIA physics tunes, varying the hadronization parameters [41]. The systematic uncertainty related to the reconstruction, including kinematical measurements, is estimated by varying the track segment efficiency from the nominal value of 90% to the worst case of 80%. Other systematic uncertainties in the reconstruction are subdominant, and an overall reconstruction systematic uncertainty of 20% is assigned.

The systematic uncertainties listed in Table I for ν_e are dominated by the flux uncertainty, with the hadronization and reconstruction uncertainties contributing at the 20% level. The flux uncertainty is dominant for ν_e since a significant fraction of ν_e originates from decays of charm hadrons, which have large uncertainties in their forward production. For ν_μ, the flux uncertainty is subdominant, with the hadronization and reconstruction uncertainties dominating.

Backgrounds.—The background from neutral-hadron interactions is estimated using MC simulation. The neutral-hadron MC samples are normalized to the equivalent luminosity of the data by using the number of observed and simulated muons. The final neutral-hadron samples are equivalent to ~400 times the size of the data.

Table II shows the selected number of neutral-hadron simulated events when applying the ν_e and ν_μ CC selections.

Systematic uncertainties on the neutral-hadron background estimate are evaluated by varying the incident muon energy distribution and by varying the physics lists used to model the neutral-hadron interactions in GEANT4. The incoming muon energy distribution was scaled up and down by a factor of $1 + E/(3\ \text{TeV})$ to distort the spectrum as a function of muon energy E, and the effect on the expected neutral-hadron background was evaluated. In addition, the relative change in the background was checked using the physics list QGSP_BERT [42] to model the hadron interactions instead of the FTFP_BERT physics list. From these studies, a systematic uncertainty of 100% on the expected background is assigned.

In addition to the neutral-hadron background, there is a contribution to the set of vertices retained by the ν_e and ν_μ CC selection from NC neutrino interactions. The background from NC neutrino interactions is estimated from simulated samples. None of the simulated NC events passed the ν_e CC selection, using a sample equivalent to 300 times the size of the analyzed dataset. The number of NC events expected in the analyzed dataset after the ν_μ CC selection is estimated as $0.045^{+0.004}_{-0.005}$ (flux) ± 0.003 (cross section) $^{+0.076}_{-0.024}$ (others) and $0.008^{+0.013}_{-0.004}$ (flux) ± 0.001 (cross section) $^{+0.007}_{-0.004}$ (others) for events originating from light hadrons and charm hadrons, respectively.

The total background estimates are $0.025^{+0.015}_{-0.010}$ and $0.22^{+0.09}_{-0.07}$ for the ν_e and ν_μ selections, respectively.

ν_e and ν_μ candidate events.—Four events are selected by the ν_e selection on data. The highest reconstructed electron energy from the selected ν_e CC candidates is 1.5 TeV. It is therefore the highest-energy ν_e interaction ever detected by accelerator-based experiments.

Eight events are selected by the ν_μ selection on data. The highest reconstructed muon momentum from the selected ν_μ CC candidates is 864 GeV, meaning that the ν_μ sample includes neutrinos with energy likely above 1 TeV, far higher than from previous accelerator-based neutrino studies.

Example event displays of ν_e and ν_μ candidates are shown in Fig. 3. As expected, both events exhibit a back-to-back topology between the lepton candidate and the other tracks in the vertex.

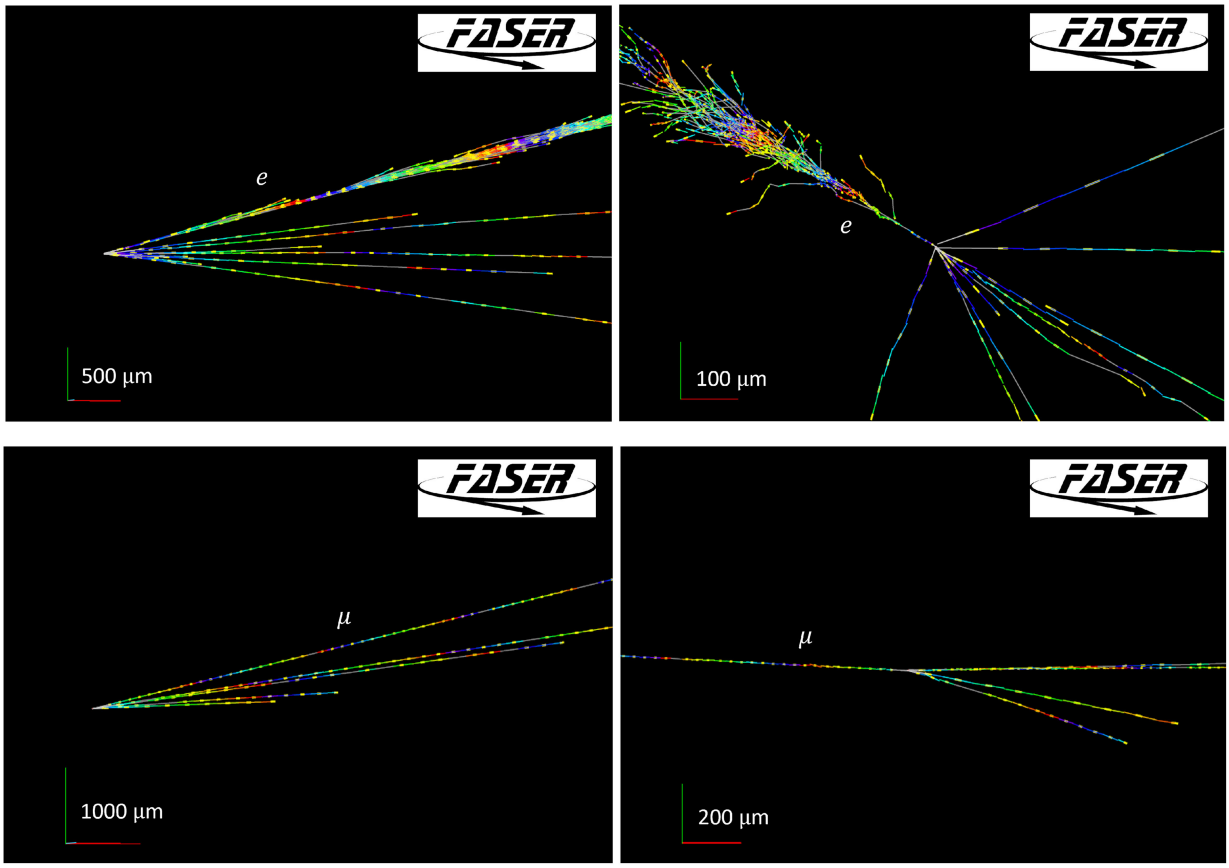

FIG. 3. Event displays of one of the ν_e CC candidate events (top) and one of the ν_μ CC candidate events (bottom). In each panel, the right-handed coordinate axes are shown in the bottom left, with red, green, and blue axes indicating the x (horizontal), y (vertical), and z (beam) directions, respectively. The right panels show views transverse to the beam direction, and so the blue axes are not visible. The left panels are slightly rotated views, with the blue axes barely visible, to show the longitudinal development of the event. Yellow line segments show the trajectories of charged particles in the emulsion films. The other colored lines are interpolations, with the colors indicating the longitudinal depth in the detector.

The expected number of neutrino signal events satisfying the selections are in the range 1.1–3.3 (for ν_e CC) and 6.5–12.4 (for ν_μ CC), where the range covers the uncertainties listed in Table I. The observed number of interactions is consistent with standard model predictions.

The statistical significance of the observation of ν_e and ν_μ is estimated by considering the confidence level for excluding the null hypothesis (background only). Based on the probability density function (PDF) for the background, 10^{10} pseudoexperiments were generated. The neutral-hadron background was generated following separate Poisson distributions for each neutral hadron species considered, with a Gaussian-distributed systematic uncertainty of 100% included. The background from neutrino NC events was generated from a Poisson distribution, with systematic uncertainties included via Gaussian-distributed nuisance parameters [separately for the uncertainties from the light hadron ($\lambda_{\text{light hadron}}$) and charm hadron ($\lambda_{\text{charm hadron}}$) neutrino flux and the experimental uncertainties (λ_{syst})].

A random value, N, was calculated following the total background PDF, and the number of pseudoexperiments with $N \geq N_{\text{obs}}$ was counted, where N_{obs} is the number of observed neutrino events. Based on the fraction of cases with $N \geq N_{\text{obs}}$, observed p values of 8.8×10^{-8} for ν_e and 5.7×10^{-9} are obtained, corresponding to significances of 5.2σ for ν_e and 5.7σ for ν_μ for the exclusion of the null hypothesis. The expected significance is estimated with pseudoexperiments with the signal expectation from the baseline flux model to be 3.3σ for ν_e and 6.4σ for ν_μ.

ν_e and ν_μ cross sections.—The number of observed neutrino events can be described as

$$N_{\text{obs}} = \frac{L\rho l}{m_{\text{nucleon}}} \int \sigma(E)\phi(E)\varepsilon(E)\mathrm{d}A\mathrm{d}E,$$

where L is the luminosity, ρ is the density of tungsten (19.3 g/cm^3), l is the thickness of the tungsten plates, m_{nucleon} is the mass of the nucleon, $\sigma(E)$ is the cross section, $\phi(E)$ is the neutrino flux at the detector integrated

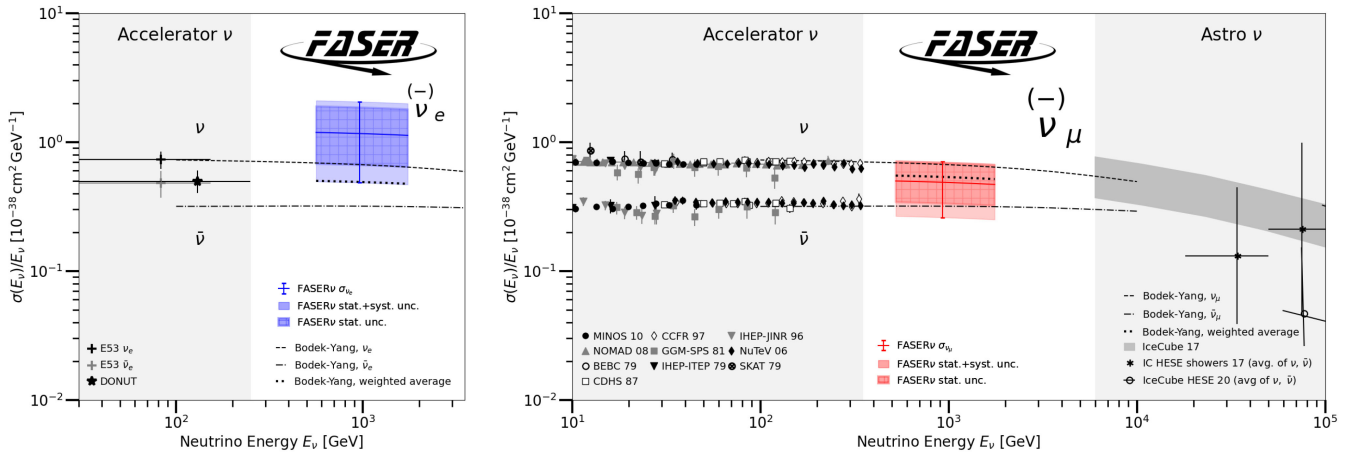

FIG. 4. The measured cross section per nucleon for ν_e (left) and ν_μ (right). The dashed contours labeled "Bodek-Yang" are cross sections predicted by the Bodek-Yang model, as implemented in GENIE. Note that the displayed experiments do not all use the same targets.

over the transverse area A and the energy E, and $\varepsilon(E)$ is the detection efficiency.

The ν_e and ν_μ CC cross sections are measured in a single energy bin. The ratio between the cross sections evaluated with the GENIE simulation (σ_{theory}) and with the observed data is defined as a factor α as described by $\sigma_{\text{obs}} = \alpha\sigma_{\text{theory}}$, assuming that α is common for neutrino and antineutrino interactions. The energy range for σ_{theory} was defined to contain 68% of reconstructed neutrinos using the baseline models, which is 560–1740 and 520–1760 GeV for ν_e and ν_μ, respectively.

The PDF of α from a Bayesian method [43] can be calculated by integrating the product of the likelihood $\mathcal{L}$ and the prior probability distribution of the nuisance parameters π. The likelihood $\mathcal{L}$ is constructed using the parameters N_{obs}, α, $\lambda_{\text{light hadron}}$, $\lambda_{\text{charm hadron}}$, and λ_{syst} that were defined in the previous section, the nuisance parameters for each neutral-hadron background and its systematic uncertainty, and the nuisance parameters for the NC background. The prior distribution π is flat and assumed to be 1 except for unphysical values of the parameters where it is 0. The posterior is obtained with a Markov chain MC with the Metropolis-Hastings algorithm [44].

The α parameter is measured to be $2.4^{+1.8}_{-1.4}$ (0.9 ± 0.4) for ν_e (ν_μ), respectively, where statistical and systematic uncertainties are combined. The statistical uncertainty is $^{+1.4}_{-1.0}$ ($^{+0.4}_{-0.3}$), which dominates the uncertainty of the measurement. The next most important component is the flux uncertainty, estimated in a fit where only the flux nuisance parameter is free and equal to $^{+0.4}_{-0.8}$ ($^{+0.03}_{-0.08}$), after quadratically subtracting the statistical uncertainty. The other systematic uncertainties are $^{+0.9}_{-0.7}$ ($^{+0.3}_{-0.2}$). The sum of these individual uncertainties should include correlations to result in the total uncertainty. The energy-independent part of the interaction cross sections per nucleon, $\sigma_{\text{obs}}/E_\nu$, is measured over the considered energy ranges to be $(1.2^{+0.8}_{-0.7}) \times 10^{-38}$ cm^2 GeV^{-1} for ν_e and $(0.5 \pm 0.2) \times 10^{-38}$ cm^2 GeV^{-1} for ν_μ. Figure 4 shows the measured cross sections, together with those obtained by other experiments [45–69]. The measured value of σ_{obs} is shown as the blue curved line for ν_e and the red curved line for ν_μ. The weighted average of the GENIE-predicted cross section is also shown, assuming the ratio of the incoming neutrino to antineutrino fluxes to be 1.04 for ν_e and 0.61 for ν_μ.

Conclusions.—First results from the search for high-energy electron and muon neutrino interactions in the FASERν tungsten-emulsion detector of the FASER experiment have been presented. The analysis uses a subset of the FASERν volume, corresponding to a target mass of 128.6 kg, exposed to 9.5 fb^{-1} of LHC pp collisions during the summer of 2022. Selections are applied to retain reconstructed vertices consistent with high-energy ν_e and ν_μ CC interactions, while minimizing the background from neutral-hadron interactions. Four electron neutrino interaction candidate events are observed, with an expected background of $0.025^{+0.015}_{-0.010}$, leading to a statistical significance of 5.2 standard deviations. This represents the first direct observation of electron neutrinos produced at a particle collider. Eight muon neutrino interaction candidate events are also found, with an expected background of $0.22^{+0.09}_{-0.07}$, leading to a statistical significance of 5.7 standard deviations. The interaction cross section per nucleon is measured over an unexplored energy range of 560–1740 GeV for ν_e and 520–1760 GeV for ν_μ. In these energy ranges, the neutrino-antineutrino combined cross sections, $\sigma_{\text{obs}}/E_\nu$, are constrained to be $(1.2^{+0.8}_{-0.7}) \times 10^{-38}$ cm^2 GeV^{-1} for ν_e and $(0.5 \pm 0.2) \times 10^{-38}$ cm^2 GeV^{-1} for ν_μ, both consistent with the cross section predictions of the standard model. These results demonstrate the capability to study flavor-tagged neutrino interactions at TeV

energies with the FASERν emulsion-based detector at the LHC.

We thank Nicolas Berger for reviewing the statistical analysis used, Mauricio Bustamante for providing the digitized neutrino cross section data, and Saya Yamamoto for supporting the preparation of emulsion films. We thank CERN for the excellent performance of the LHC and the technical and administrative staff members at all FASER institutions for their contributions to the success of the FASER experiment. We thank the ATLAS Collaboration for providing us with accurate luminosity estimates for the run 3 LHC pp collision data. We also thank the CERN STI group for providing detailed FLUKA simulations of the muon fluence along the LOS, the CERN EN-HE group for their help with the installation and removal of the FASERν detector, and the CERN EP department for the refurbishment of the CERN dark room, used for the preparation and development of the FASERν emulsion. This work was supported in part by Heising-Simons Foundation Grants No. 2018-1135, No. 2019-1179, and No. 2020-1840, Simons Foundation Grant No. 623683, U.S. National Science Foundation Grants No. PHY-2111427, No. PHY-2110929, and No. PHY-2110648, JSPS KAKENHI Grants No. 19H01909, No. 22H01233, No. 20K23373, No. 23H00103, No. 20H01919, and No. 21H00082, the joint research program of the Institute of Materials and Systems for Sustainability, ERC Consolidator Grant No. 101002690, BMBF Grant No. 05H20PDRC1, DFG EXC 2121 Quantum Universe Grant No. 390833306, Royal Society Grant No. URF\R1\201519, UK Science and Technology Funding Councils Grant No. ST/T505870/1, the National Natural Science Foundation of China, Tsinghua University Initiative Scientific Research Program, and the Swiss National Science Foundation.

Appendix A: Reconstructed data quality.—This appendix describes the reconstructed data quality of the analyzed volume, checked using penetrating muon tracks. Figure 5 shows the measured position resolution of 0.3 μm in a plane transverse to the beam. The track hit efficiency in each film was measured to be greater than 90% in the reconstructed volumes, corresponding to an efficiency greater than 99.98% for detecting tracks with at least three hits in seven films.

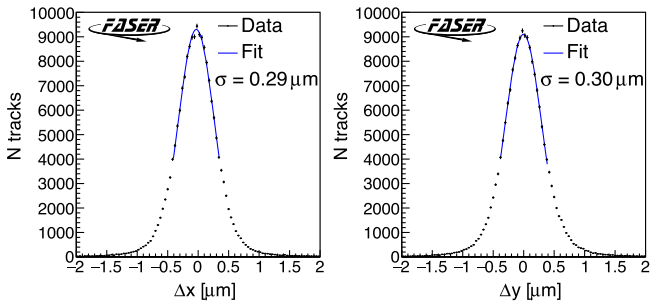

FIG. 5. Distributions of the position deviation of the track hits with respect to a linear-fit line for the reconstructed tracks, measured in a typical subvolume of the FASERν data. The blue line shows a Gaussian fit to the data, giving a position resolution of 0.29–0.30 μm.

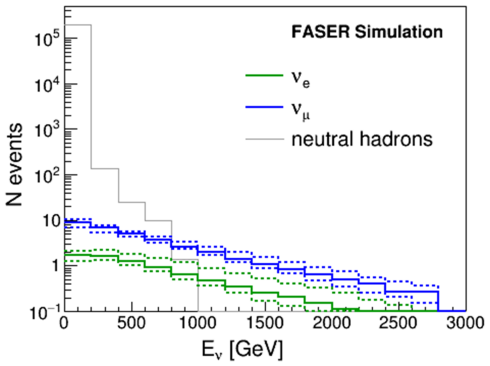

FIG. 6. Simulation of the energy spectrum of electron (solid green curve) and muon neutrinos (solid blue curve) within the analyzed detector volume are shown for an integrated luminosity of 9.5 fb^{-1}. The dashed lines envelope the predictions from different generators; for more details, see text. The energy spectrum of neutral hadrons (gray curve) is also shown.

Appendix B: Expected energy spectrum of interacting neutrinos.—This appendix describes the expected energy spectrum of interacting neutrinos, as well as that of the neutral-hadron backgrounds; these are shown in Fig. 6. The expected numbers of neutrino interaction events before selection cuts are listed in Table III.

Appendix C: Resolutions of electron energy and muon momentum measurements.—This appendix describes the electron energy and muon momentum measurement resolutions used for the event selection. The energy reconstruction algorithm performance was tested for electrons in the ν_e MC simulation (Fig. 7), showing a resolution of around 25% at 200 GeV and between 25% and 40% at higher energies.

The resolution, as quantified by the rms of the distribution of the difference between the true momentum and reconstructed momentum, is around 30% at 200 GeV and reaches 50% at higher energies; see Fig. 8. The track momentum assessment performance is validated with data by studying the momenta of long tracks: they are split into

TABLE III. Expected number of CC and NC neutrino interaction events with the analyzed detector volume, along with the uncertainty from the neutrino flux.

$\nu_e + \bar{\nu}_e$ CC	$\nu_\mu + \bar{\nu}_\mu$ CC	$\nu_\tau + \bar{\nu}_\tau$ CC	NC
$8.5^{+4.3}_{-1.8}$	$43.6^{+4.7}_{-5.2}$	$0.12^{+0.22}_{-0.05}$	$16.5^{+3.0}_{-2.1}$

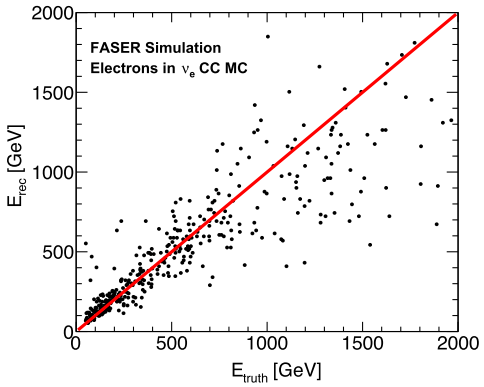

FIG. 7. The reconstructed electron energy versus the true energy in ν_e CC MC simulation.

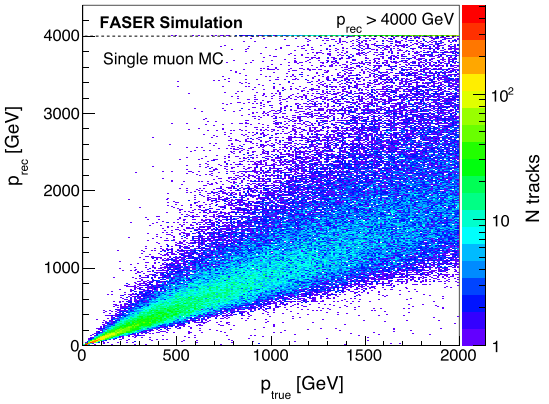

FIG. 8. Reconstructed momenta versus true momenta in simulated muon tracks with a flat momentum distribution from 1 to 2000 GeV.

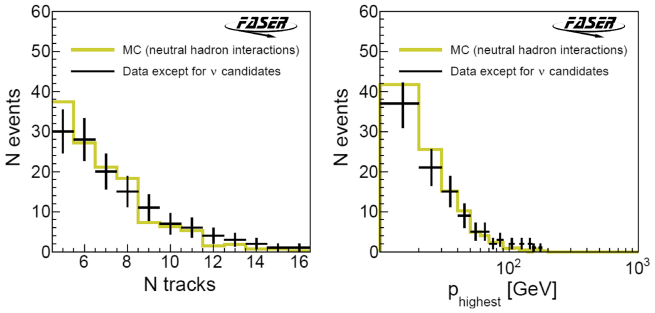

FIG. 9. MC simulation distributions of track multiplicity (left) and momentum of the highest momentum track (right) from neutral-hadron interactions vertices. The observed events in the data sample (except for neutrino candidate events) are shown in black. The MC simulation distributions are normalized to the number of events observed in the data with the normalization factor of 0.57.

two tracks, and the reconstructed momenta of the two halves is compared, resulting in a reasonable agreement.

Appendix D: Validation of the modeling of the neutral-hadron background.—This appendix describes the validation of the modeling of the neutral-hadron background, using the initial neutral-vertex sample of data (before the high-energy electron or muon selection is applied), which is dominated by neutral-hadron interactions. For this validation study, only a part of the analyzed volume (150 tungsten plates from film 7 to 156) was used. The expected number of hadron

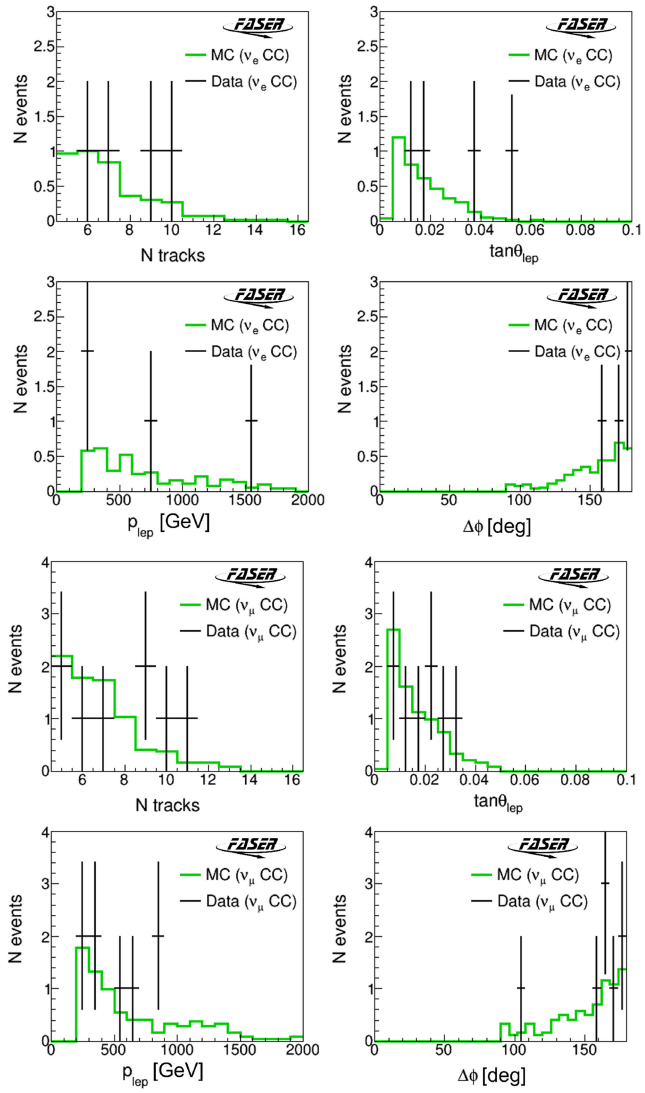

FIG. 10. MC simulation distributions of the track multiplicity (N tracks), lepton angle ($\tan\theta_{\mathrm{lep}}$), lepton momentum ($p_{\mathrm{lep}}$), and $\Delta\phi$ for the ν_e CC (top four figures) and ν_μ CC (bottom four figures) signal that passed the selection criteria. The observed ν_e CC and ν_μ CC candidate events in the data sample are shown in black. The MC simulation distributions are normalized to the number of observed events with the normalization factor of 2.3 (0.9) for ν_e (ν_μ).

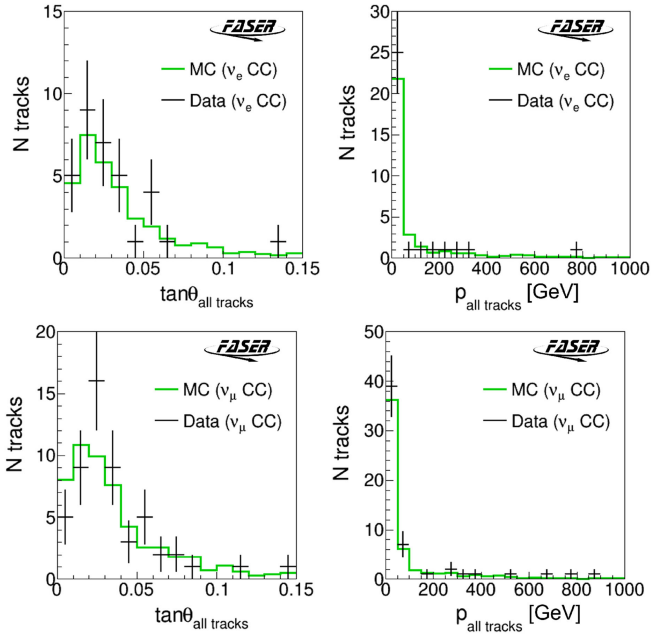

FIG. 11. MC simulation distributions of track angle and momentum from vertices of the ν_e CC (top) and ν_μ CC (bottom) signal. The observed ν_e CC and ν_μ CC candidate events in the data sample are shown in black. The MC simulation distributions are normalized to the number of observed tracks.

interaction vertices is 246, while the number of neutral vertices in the data sample is 139. Figure 9 shows a comparison of the number of tracks in the vertex, and the reconstructed momentum of the highest momentum track, between the neutral-hadron MC and the data. For the comparison, the MC distributions are normalized to the same number of vertices as observed in the data. The neutrino candidates that satisfy the event selection are excluded from the data for this comparison. The distribution shapes are well modeled in the simulation, and the number of interactions is found to be compatible at better than the 50% level, with more neutral-hadron interactions predicted in the MC than observed in the data.

Appendix E: Properties of the ν_e and ν_μ CC candidate events.—This appendix describes the properties of the selected vertices compared with the expectations from ν_e CC and ν_μ CC simulation (Fig. 10) and for the properties of the individual tracks forming the vertices (Fig. 11). In general, the simulation describes the data well for both the ν_e and ν_μ selections.

*Corresponding author: ariga@artsci.kyushu-u.ac.jp
†faser-publications@cern.ch

[1] J. L. Feng, I. Galon, F. Kling, and S. Trojanowski, Forward search experiment at the LHC, Phys. Rev. D **97**, 035001 (2018).
[2] FASER Collaboration, Letter of intent for FASER: Forward search experiment at the LHC, arXiv:1811.10243.
[3] FASER Collaboration, Technical proposal for FASER: Forward search experiment at the LHC, arXiv:1812.09139.
[4] L. Evans and P. Bryant, LHC Machine, J. Instrum. **3**, S08001 (2008).
[5] FASER Collaboration, Detecting and studying high-energy collider neutrinos with FASER at the LHC, Eur. Phys. J. C **80**, 61 (2020).
[6] FASER Collaboration, Technical proposal: FASERν, arXiv:2001.03073.
[7] FASER Collaboration, The FASER detector, J. Instrum. **19**, P05066 (2024).
[8] FASER Collaboration, First neutrino interaction candidates at the LHC, Phys. Rev. D **104**, L091101 (2021).
[9] FASER Collaboration, First direct observation of collider neutrinos with FASER at the LHC, Phys. Rev. Lett. **131**, 031801 (2023).
[10] C. Ahdida *et al.* (SHiP Collaboration), SND@LHC, arXiv:2002.08722.
[11] G. Acampora *et al.* (SND@LHC Collaboration), SND@LHC: The scattering and neutrino detector at the LHC, J. Instrum. **19**, P05067 (2024).
[12] R. Albanese *et al.* (SND@LHC Collaboration), Observation of collider muon neutrinos with the SND@LHC experiment, Phys. Rev. Lett. **131**, 031802 (2023).
[13] ν_τ CC events are not considered in this analysis due to the small number of expected events in the analyzed sample, as shown in Table III of Appendix B.
[14] L. A. Anchordoqui *et al.*, The forward physics facility: Sites, experiments, and physics potential, Phys. Rep. **968**, 1 (2022).
[15] J. L. Feng *et al.*, The forward physics facility at the high-luminosity LHC, J. Phys. G **50**, 030501 (2023).
[16] J. M. Cruz-Martinez, M. Fieg, T. Giani, P. Krack, T. Mäkelä, T. R. Rabemananjara, and J. Rojo, The LHC as a neutrino-ion collider, Eur. Phys. J. C **84**, 369 (2024).
[17] F. Kling, T. Mäkelä, and S. Trojanowski, Investigating the fluxes and physics potential of LHC neutrino experiments, Phys. Rev. D **108**, 095020 (2023).
[18] C. Wilkinson and A. Garcia Soto, Low-ν method with LHC neutrinos, Phys. Rev. D **109**, 033010 (2024).
[19] A. Ariga, T. Ariga, G. De Lellis, A. Ereditato, and K. Niwa, *Nuclear Emulsions* (Springer, Cham, 2020), pp. 383–438, 10.1007/978-3-030-35318-6_9.
[20] ATLAS Collaboration, Preliminary analysis of the luminosity calibration of the ATLAS 13.6 TeV data recorded in 2022, Report No. ATL-DAPR-PUB-2023-001, 2023, http://cds.cern.ch/record/2853525.
[21] ATLAS Collaboration, Luminosity determination in pp collisions at $\sqrt{s} = 13$ TeV using the ATLAS detector at the LHC, Eur. Phys. J. C **83**, 982 (2023).
[22] G. Avoni *et al.*, The new LUCID-2 detector for luminosity measurement and monitoring in ATLAS, J. Instrum. **13**, P07017 (2018).
[23] A Cartesian coordinate system is used with the z axis running along the LOS from the ATLAS collision point to FASER, the y axis pointing vertically upward, and the x axis pointing horizontally to the center of the LHC ring. The angle ϕ is the azimuthal angle in the (x-y) plane, and θ is the polar angle measured from the beam direction.

[24] M. Yoshimoto, T. Nakano, R. Komatani, and H. Kawahara, Hyper-track selector nuclear emulsion readout system aimed at scanning an area of one thousand square meters, Prog. Theor. Exp. Phys. **2017**, 103H01 (2017).

[25] S. Aoki *et al.* (DsTau Collaboration), DsTau: Study of tau neutrino production with 400 GeV protons from the CERN-SPS, J. High Energy Phys. 01 (2020) 033.

[26] F. Kling and L. J. Nevay, Forward neutrino fluxes at the LHC, Phys. Rev. D **104**, 113008 (2021).

[27] FASER Collaboration, Neutrino rate predictions for FASER, arXiv:2402.13318.

[28] T. Pierog, I. Karpenko, J. M. Katzy, E. Yatsenko, and K. Werner, EPOS LHC: Test of collective hadronization with data measured at the CERN Large Hadron Collider, Phys. Rev. C **92**, 034906 (2015).

[29] S. Ostapchenko, Monte Carlo treatment of hadronic interactions in enhanced Pomeron scheme: I. QGSJET-II model, Phys. Rev. D **83**, 014018 (2011).

[30] C. Bierlich *et al.*, A comprehensive guide to the physics and usage of PYTHIA8.3, SciPost Phys. Codebases **2022**, 8 (2022).

[31] M. Fieg, F. Kling, H. Schulz, and T. Sjöstrand, Tuning PYTHIA for forward physics experiments, Phys. Rev. D **109**, 016010 (2024).

[32] L. Buonocore, F. Kling, L. Rottoli, and J. Sominka, Predictions for neutrinos and new physics from forward heavy hadron production at the LHC, Eur. Phys. J. C **84**, 363 (2024).

[33] C. Andreopoulos *et al.*, The GENIE neutrino Monte Carlo generator, Nucl. Instrum. Methods Phys. Res., Sect. A **614**, 87 (2010).

[34] C. Andreopoulos, C. Barry, S. Dytman, H. Gallagher, T. Golan, R. Hatcher, G. Perdue, and J. Yarba, The GENIE neutrino Monte Carlo generator: Physics and user manual, arXiv:1510.05494.

[35] S. Agostinelli *et al.* (GEANT4 Collaboration), GEANT4–a simulation toolkit, Nucl. Instrum. Methods Phys. Res., Sect. A **506**, 250 (2003).

[36] A. Ferrari, P. R. Sala, A. Fasso, and J. Ranft, FLUKA: A multi-particle transport code (Program version 2005), 10.5170/CERN-2005-010.

[37] G. Battistoni *et al.*, Overview of the FLUKA code, Ann. Nucl. Energy **82**, 10 (2015).

[38] T. Kobayashi, Y. Komori, K. Yoshida, K. Yanagisawa, J. Nishimura, T. Yamagami, Y. Saito, N. Tateyama, T. Yuda, and R. J. Wilkes, Observations of high energy cosmic-ray electrons from 30 GeV to 3 TeV with emulsion chambers, Astrophys. J. **760**, 146 (2012).

[39] F. Juget, Electromagnetic shower reconstruction with emulsion films in the OPERA experiment, J. Phys. Conf. Ser. **160**, 012033 (2009).

[40] K. Kodama *et al.*, Momentum measurement of secondary particle by multiple Coulomb scattering with emulsion cloud chamber in DONuT experiment, Nucl. Instrum. Methods Phys. Res., Sect. A **574**, 192 (2007).

[41] J. Tena-Vidal *et al.* (GENIE Collaboration), Hadronization model tuning in GENIE v3, Phys. Rev. D **105**, 012009 (2022).

[42] J. Allison *et al.*, Recent developments in GEANT4, Nucl. Instrum. Methods Phys. Res., Sect. A **835**, 186 (2016).

[43] P. A. Zyla *et al.* (Particle Data Group), Review of particle physics, Prog. Theor. Exp. Phys. **2020**, 083C01 (2020).

[44] P. Gregory, *Markov Chain Monte Carlo* (Cambridge University Press, Cambridge, England, 2005), pp. 312–351, 10.1017/CBO9780511791277.013.

[45] C. Baltay *et al.*, $\nu_\mu - \nu_e$ universality in charged current neutrino interactions, Phys. Rev. D **41**, 2653 (1990).

[46] K. Kodama *et al.* (DONuT Collaboration), Final tau-neutrino results from the DONuT experiment, Phys. Rev. D **78**, 052002 (2008).

[47] P. Adamson *et al.* (MINOS Collaboration), Neutrino and antineutrino inclusive charged-current cross section measurements with the MINOS near detector, Phys. Rev. D **81**, 072002 (2010).

[48] Q. Wu *et al.* (NOMAD Collaboration), A precise measurement of the muon neutrino-nucleon inclusive charged current cross-section off an isoscalar target in the energy range $2.5 < E_\nu < 40$ GeV by NOMAD, Phys. Lett. B **660**, 19 (2008).

[49] K. Abe *et al.* (T2K Collaboration), Measurement of the inclusive ν_μ charged current cross section on carbon in the near detector of the T2K experiment, Phys. Rev. D **87**, 092003 (2013).

[50] K. Abe *et al.* (T2K Collaboration), Measurement of the ν_μ charged-current quasielastic cross section on carbon with the ND280 detector at T2K, Phys. Rev. D **92**, 112003 (2015).

[51] K. Abe *et al.* (T2K Collaboration), Measurement of the inclusive ν_μ charged current cross section on iron and hydrocarbon in the T2K on-axis neutrino beam, Phys. Rev. D **90**, 052010 (2014).

[52] C. Anderson *et al.* (ArgoNeuT Collaboration), First measurements of inclusive muon neutrino charged current differential cross sections on argon, Phys. Rev. Lett. **108**, 161802 (2012).

[53] R. Acciarri *et al.* (ArgoNeuT Collaboration), Measurements of inclusive muon neutrino and antineutrino charged current differential cross sections on argon in the NuMI antineutrino beam, Phys. Rev. D **89**, 112003 (2014).

[54] S. J. Barish *et al.*, Study of neutrino interactions in hydrogen and deuterium: Inelastic charged current reactions, Phys. Rev. D **19**, 2521 (1979).

[55] J. G. H. de Groot *et al.*, Inclusive interactions of high-energy neutrinos and anti-neutrinos in iron, Z. Phys. C **1**, 143 (1979).

[56] D. C. Colley *et al.*, Cross-sections for charged current neutrino and anti-neutrino interactions in the energy range 10-GeV to 50-GeV, Z. Phys. C **2**, 187 (1979).

[57] N. J. Baker, P. L. Connolly, S. A. Kahn, M. J. Murtagh, R. B. Palmer, N. P. Samios, and M. Tanaka, Total cross-sections for muon-neutrino N and muon-neutrino P charged current interactions in the 7-ft bubble chamber, Phys. Rev. D **25**, 617 (1982).

[58] J. P. Berge *et al.*, Total neutrino and anti-neutrino charged current cross-section measurements in 100-GeV, 160-GeV and 200-GeV narrow band beams, Z. Phys. C **35**, 443 (1987).

[59] W. G. Seligman, A next-to-leading order QCD analysis of neutrino-iron structure functions at the Tevatron, Ph.D. thesis, Nevis Labs, Columbia University, 1997, 10.2172/1421736.

[60] S. Ciampolillo *et al.* (Gargamelle Neutrino Propane and Aachen-Brussels-CERN-Ecole Poly-Orsay-Padua

Collaborations), Total cross-section for neutrino charged current interactions at 3-GeV and 9-GeV, Phys. Lett. **84B**, 281 (1979).

[61] J. G. Morfin *et al.* (Gargamelle SPS Collaboration), Total cross-sections and nucleon structure functions in the Gargamelle SPS neutrino/anti-neutrino experiment, Phys. Lett. **104B**, 235 (1981).

[62] A. I. Mukhin, V. F. Perelygin, K. E. Shestermanov, A. A. Volkov, A. S. Vovenko, and V. P. Zhigunov, Energy dependence of total cross-sections for neutrino and anti-neutrino interactions at energies below 35-GeV, Sov. J. Nucl. Phys. **30**, 528 (1979).

[63] V. B. Anikeev *et al.*, Total cross-section measurements for muon-neutrino, anti-muon-neutrino interactions in 3–30 GeV energy range with IHEP-JINR neutrino detector, Z. Phys. C **70**, 39 (1996).

[64] M. Tzanov *et al.* (NuTeV Collaboration), Precise measurement of neutrino and anti-neutrino differential cross sections, Phys. Rev. D **74**, 012008 (2006).

[65] Y. Nakajima *et al.* (SciBooNE Collaboration), Measurement of inclusive charged current interactions on carbon in a few-GeV neutrino beam, Phys. Rev. D **83**, 012005 (2011).

[66] D. S. Baranov *et al.*, Measurements of the $\nu_\mu N$ total cross-section at 2–30 GeV in skat neutrino experiment, Phys. Lett. **81B**, 255 (1979).

[67] M. G. Aartsen *et al.* (IceCube Collaboration), Measurement of the multi-TeV neutrino cross section with IceCube using Earth absorption, Nature (London) **551**, 596 (2017).

[68] M. Bustamante and A. Connolly, Extracting the energy-dependent neutrino-nucleon cross section above 10 TeV using IceCube showers, Phys. Rev. Lett. **122**, 041101 (2019).

[69] R. Abbasi *et al.* (IceCube Collaboration), Measurement of the high-energy all-flavor neutrino-nucleon cross section with IceCube, Phys. Rev. D **104**, 022001 (2021).